Chapter 3

Femtosecond Pulse Shaping with Liquid Crystal Modulators

Many approaches in femtosecond pulse shaping were dedicated to the synthesis of laser waveforms by spectral filtering of a spatially dispersed frequency spectrum. This chapter describes the most successful and widely employed method, also used in this work, to shape femtosecond laser pulses: pulse shaping with spatial light modulators (SLMs). This method is the key part in feedback control experiments. The central element is a commercially available spatial light modulator based on liquid crystals (LC), which permits (re)programmable waveform generation by computer control.

A short theoretical introduction of shaped femtosecond pulses is followed by the description of the pulse shaper itself. The working principle of the LC SLM used in this work, together with its implementation in a pulse shaping apparatus, is discussed in the next section. A large number of other experimental pulse shaping techniques is based on other methods. A few of them are mentioned at the end of the chapter and a comparison is given.

3.1 Shaped Femtosecond Laser Pulses

The available control electronics are too slow for a modulation of a laser pulse in the femtosecond time domain. Thus it is required to modulate the amplitude and the phase of the laser field in the frequency domain. The time and frequency representation of a femtosecond laser pulse (i.e. its intensity and/or phase profile) are connected by the Fourier transform.

Using the Fourier transform, the complex spectral intensity $\tilde{E}(\omega)$ can be described by

$$\tilde{E}(\omega) = \int_{-\infty}^{+\infty} E(t)e^{-i\omega t}dt, \tag{3.1}$$

where $E(t)$ is the temporal electric field of a laser pulse. The electric field in the time domain $E(t)$ can be written by using the inverse Fourier transform

$$E(t) = \frac{1}{2\pi}\int_{-\infty}^{+\infty} \tilde{E}(\omega)e^{i\omega t}d\omega \tag{3.2}$$

The complex quantity $\tilde{E}(\omega)$ has values for both positive and negative frequencies. Hence the following complex quantities are introduced:

$$\tilde{E}^{+}(t) = \frac{1}{2\pi}\int_{0}^{+\infty} \tilde{E}(\omega)e^{i\omega t}d\omega \tag{3.3}$$

$$\tilde{E}^{-}(t) = \frac{1}{2\pi}\int_{-\infty}^{0} \tilde{E}(\omega)e^{i\omega t}d\omega \tag{3.4}$$

Since the negative value $\tilde{E}^{-}(t)$ is not a measurable quantity, it does not have a physical meaning. The original electric field is reconstructed from the equations (3.3) and (3.4):

$$E(t) = \tilde{E}^{+}(t) + \tilde{E}^{-}(t). \tag{3.5}$$

The real complex spectral description of the electric field is also introduced only for positive frequencies, from the same reason as for the temporal electric field

$$\tilde{E}^{+}(\omega) = \begin{cases} \tilde{E}(\omega) & \text{if} \quad \omega \geq 0 \\ 0 & \text{if} \quad \omega < 0 \end{cases}$$

whereby each $\tilde{E}^{+}(t)$ and $\tilde{E}^{+}(\omega)$ is the Fourier transform of the other (see equations (3.1) and (3.2)). Certainly, the complex form $\tilde{E}(\omega)$ is reconstructed as $\tilde{E}(\omega) = \tilde{E}^{+}(\omega) + \tilde{E}^{-}(\omega)$.

3.1.1 Phase Modulation in Temporal Domain

The time-dependent complex electric field $\tilde{E}^{+}(t)$ can be separated in

$$\tilde{E}^{+}(t) = T(t)e^{-i\Theta(t)} \tag{3.6}$$

where T(t) is the temporal amplitude and $\Theta(t)$ is the temporal phase factor. For pulses having a few optical cycles[1], because $\Delta\omega \ll \omega_0$, where $\Delta\omega$ is the

[1]This approximation is also called Slow Varying Envelope Approximation.

spectral full-width at half-maximum, the phase factor $\Theta(t)$ can be written as a function of phase $\varphi(t)$ and carrier frequency ω_0 :

$$\tilde{E}^+(t) = T(t)e^{-i\varphi(t)}e^{\omega_0 t}. \tag{3.7}$$

The time derivative of the phase factor $\Theta(t)$ gives the instantaneous frequency[2] as a function of time [21]

$$\frac{d\Theta(t)}{dt} = \omega(t) = \omega_0 - \frac{d\varphi(t)}{dt}. \tag{3.8}$$

Developing the phase $\varphi(t)$ around t_0 in Taylor series gives a closer look at the chirp in time domain:

$$\varphi(t) = \varphi(t_0) + \frac{d\varphi(t)}{dt}\bigg|_{t_0}(t-t_0) + \frac{1}{2}\frac{d^2\varphi(t)}{dt^2}\bigg|_{t_0}(t-t_0)^2 + \cdots \tag{3.9}$$

or

$$\varphi(t) = a_0 + a_1(t-t_0) + \frac{1}{2}\cdot a_2(t-t_0)^2 + \cdots \tag{3.10}$$

The quantity $a_0 = \varphi(t_0)$ represents the constant phase of the electric field which determines the relative position of the fast oscillations of the electric field with respect to the pulse envelope. The linear variation of the phase in time $\varphi(t)$ is described by the term $a_1 = \frac{d\varphi(t)}{dt}\big|_{t_0}$ which gives the shift of the carrier frequency ω_0. For a transform-limited pulse the temporal phase depends linearly with time: $\varphi(t) = a_0 + a_1 t$. The quadratic term $a_2 = \frac{d^2\varphi(t)}{dt^2}\big|_{t_0}$ gives the linear chirp, i.e. the linear variation of the instantaneous frequency with time (see equation (3.8)). If $\frac{d^2\varphi(t)}{dt^2}\big|_{t_0} < 0$ the instantaneous frequency increases with time; this is the case of a positive chirp or *upchirp*. The opposite situation, when $\frac{d^2\varphi(t)}{dt^2}\big|_{t_0} > 0$, i.e. the instantaneous frequency decreases in time, is described as a negative chirp or *downchirp*. The linear chirp is measured in fs^{-2}. For $\frac{d^3\varphi(t)}{dt^3}\big|_{t_0}$ and higher orders, the terms give the quadratic and higher order chirps.

An example of nonlinear phase modulation in temporal domain of an unchirped femtosecond pulse is the so-called self-phase modulation (SPM). The modulation phase term is described as [14]

[2]The equation (3.8) is sometimes controversial in the femtosecond community due to the minus sign, present in Ref. [21]. Other references use the plus sign, like Ref. [14]. In fact the definition is true in both cases as long the initial convention of defining a positive or negative chirp, respectively, remains valid throughout the study. For example it is known that a positive chirp is generated by a material with "normal" or "positive" dispersion.

$$\Psi(t) = -\frac{2\pi}{\lambda_0} n(t) d \tag{3.11}$$

where λ_0 is the central wavelength of the pulse, d is the thickness of the optical medium wherethrough the pulse propagates and $n(t)$ the time-dependent refractive index, caused by the intensity change in the pulse envelope. This phenomenon leads to a change in the spectrum without affecting the time duration of the pulse.

3.1.2 Phase Modulation in Spectral Domain

The most common case of a spectral phase modulation is the dispersion in a transparent material (e.g. optical glass), which posses a time independent refractive index $n(\omega)$. This phenomenon does not change the pulse spectrum. The phase term [32]

$$\Psi(\omega) = \frac{2\pi}{\lambda_0} n(\omega) d \tag{3.12}$$

is responsible for modulation of the electric field $\tilde{E}^+(\omega)$, where d is the thickness of the optical medium. After propagating through such a medium, the frequency components within the pulse will disperse and travel with different time delays towards each other (have different optical paths). (This phenomenon is called G*roup* V*elocity* D*ispersion* (GVD) and was mentioned in Chapter 2, section 2.1.1.)

Hence it is of an advantage to Fourier transform the pulse in the frequency domain, to calculate the phase for each of its frequency components and then to perform an inverse Fourier transform back in the time domain.

The Taylor development of $\Psi(\omega)$ around the central frequency ω_0 is written below

$$\Psi(\omega) = \Psi(\omega_0) + \frac{d\Psi(\omega)}{d\omega}\bigg|_{\omega_0} (\omega - \omega_0) + \frac{1}{2}\frac{d^2\Psi(\omega)}{d\omega^2}\bigg|_{\omega_0} (\omega - \omega_0)^2 + \cdots \tag{3.13}$$

or

$$\Psi(t) = b_0 + b_1(\omega - \omega_0) + \frac{1}{2} b_2 (\omega - \omega_0)^2 + \cdots \tag{3.14}$$

The first term is a constant and determines the relative temporal phase of the pulse. The change of the linear coefficient $b_1 = \frac{d\Psi(\omega)}{d\omega}\big|_{\omega_0}$ results (after a Fourier transform) in a the temporal pulse shift on the time axis and gives the group delay. b_1 is responsible for varying the temporal position

of the pulse (see also equation (3.18)). The coefficient $b_2 = \frac{d^2\Psi(\omega)}{d\omega^2}\Big|_{\omega_0}$ gives the linear spectral chirp. Thus a spectral chirp of (n-1) $^{\text{th}}$ order is given by $b_n = \frac{d^n\Psi(\omega)}{d\omega^n}\Big|_{\omega_0}$.

Since shaping of the femtosecond pulses with the LC modulator takes place in the frequency domain, a short introduction is given in the next paragraph.

Similar to the temporal domain, the electric field can be separated in its envelope S(ω) and its phase $\varphi(\omega)$:

$$\tilde{E}^+_{in}(\omega) = S(\omega)e^{-i\varphi(\omega)}. \tag{3.15}$$

Here the envelope $S(\omega) = \frac{1}{\sqrt{2\epsilon_0}}\sqrt{I(\omega)}$ is calculated from the measured spectrum $I(\omega)$. The notation $\tilde{E}^+_{in}(\omega)$ was used because the input laser pulse is to be shaped after passing through the modulation filter. The modulation filter is described by the complex function

$$H(\omega) = R(\omega)e^{-i\Psi(\omega)}, \tag{3.16}$$

where $R(\omega)$ represents the amplitude filter. The phase factor $\Psi(\omega)$ is responsible for the phase delay of every frequency component and it has the form like in equation (3.14). After passing through the modulative optical element, the output electric field has the form

$$\tilde{E}^+_{out}(\omega) = H(\omega)\tilde{E}^+_{in}(\omega) = R(\omega)e^{-i\Psi(\omega)}\tilde{E}^+_{in}(\omega). \tag{3.17}$$

By inserting equation (3.14) in (3.17) and performing a Fourier transform one obtains the shape of the output electric field after passing through the modulator

$$\tilde{E}^+_{out}(t) = \frac{1}{2\pi}R_0 e^{-ib_0}e^{i\omega_o t}\int_{-\infty}^{+\infty}\tilde{E}^+_{in}(\omega)e^{-i\sum_{n=2}^{\infty}\frac{1}{n!}b_n(\omega-\omega_0)^n}e^{i(\omega-\omega_0)(t-b_1)}d\omega. \tag{3.18}$$

with the b_n coefficients taken from equation (3.14).

3.2 The Pulse Shaper

3.2.1 Liquid Crystals

Liquid crystals (LC) allow the construction of devices which operate over a wide temperature range without a precise temperature control [33]. The main

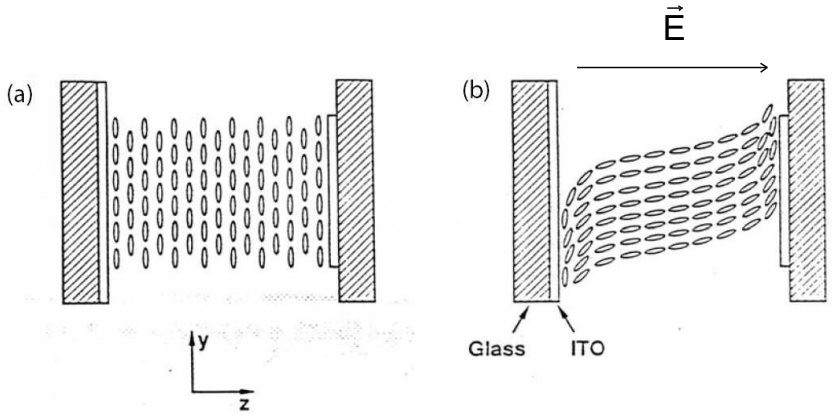

Figure 3.1: A sectional view of a liquid crystal layer between two glass plates. (a) When no voltage is applied, the LC molecules are oriented along the y-axis. (b) When voltage is applied on the ITO electrodes in the z-direction, the resulting electric field causes the tilt of the LC molecules parallel to it. This induces a change in the refraction index for the y-polarized light [4].

characteristic of the LC is that there is no defined distance between the long-stretched molecules, as in a crystal. There are different types of LC: nematic, smectic and cholesteric, which mainly differ by the LC orientation in the cell volume. In the fabrication of the programmable pulse shaping element employed in this work, nematic molecules were used. The construction of a homogeneous LC cell implies an unidirectional rubbing with a fine polishing compound (alumina or diamond). The low-viscosity LC layer is sandwiched between a pair of glass substrates. The parallel rubbing of the inner glass plate leads to a parallel alignment of the molecules with the rubbing direction[3].

The nematic molecule is optically anisotropic and its orientation can be described by the anisotropic dielectric tensor, which has as a consequence, the birefringence property. The optical axis of the molecule (extraordinary refractive index) coincides with the molecular long axis.

A nematic LC consists of a long, thin, rod-like molecules which in the absence of the electrical field are aligned with their long axes along the y-direction (see Figure 3.1). After propagating through a birefringent crystal, any circular polarized light, will split in an ordinary and an extraordinary ray, being perpendicular respectively parallel polarized with respect to the optical axis (the z-axis). When the voltage V is applied on the LC cell in

[3]A cell of *twisted nematic* molecules is obtained by rubbing the two glass plates perpendicular to each other.

the z-direction[4], electric dipoles are induced. The resulting electric forces tilt the LC molecules along z with the angle θ, causing a change in the refractive index for the y-polarized light, while the refractive index n_0 in the ordinary direction (x-axis) remains constant. The resulting wave retardance of the extraordinary ray with respect to the ordinary ray depends on the thickness d and the central wavelength λ:

$$\Gamma = 2\pi(n(\theta) - n_0)d/\lambda \quad \text{with} \quad \Gamma_{max} = 2\pi(n_e - n_0)d/\lambda, \tag{3.19}$$

whereby

$$\frac{1}{n^2(\theta(V))} = \frac{cos^2(n(\theta(V)))}{n_e^2} + \frac{sin^2(n(\theta(V)))}{n_0^2}. \tag{3.20}$$

Typical numbers are d ~ 10 μm and $n_e - n_0$ between 0.1 and 0.3. The LC masks can perform phase-only modulation, amplitude-only modulation, or both. This depends on the relative propagation of the incoming polarization, the LC axes, and the second polarizer. Details about the operation in phase and/or amplitude modulation regime are given in section 3.2.5.

3.2.2 The SLM-256

The liquid crystal spatial light modulator (SLM) used in this work is a commercially available model[5]. It consists of two linear arrays of 128 pixels each, separated by 2.2 mm, with independent control of each pixel. This allows the control of both phase and/or the amplitude independently and simultaneously (see Figure 3.2).

The two LC elements of the SLM are placed between two glass substrates (e.g. silica) coated with ITO, which is an optically transparent material but electrically conductive. One substrate is the ground plate and the second is patterned with a linear array of 128 electrodes with a width of 97 μm each that define the pixels. Each pixel in the first array is superimposed directly in front of the corresponding pixel in the second array (2×128). The 3 μm spacing between the electrodes (gaps) cannot be controlled. The filter for the gap is assumed to be constant across the whole array. The two polarizers can be glued to the glass plates or, optionally, screwed onto the mounting.

The modulator operates by modulation of polarized light. The SLM optics provide continuously variable adjustment of phase and/or amplitude. In practice the adjustment resolution is set by the electronic driver[6], which provides 4096 discrete drive levels. The electronics provide up to $V_{\max} = 10$ V

[4]Transparent ITO (Indium Tin Oxide) electrodes are coated inside the glass plates.
[5]Cambridge Research and Instrumentation (CRI, Inc.), SLM-256, Woburn, MA, U.S.A.
[6]CRI Inc., model SLM-ELT-256.

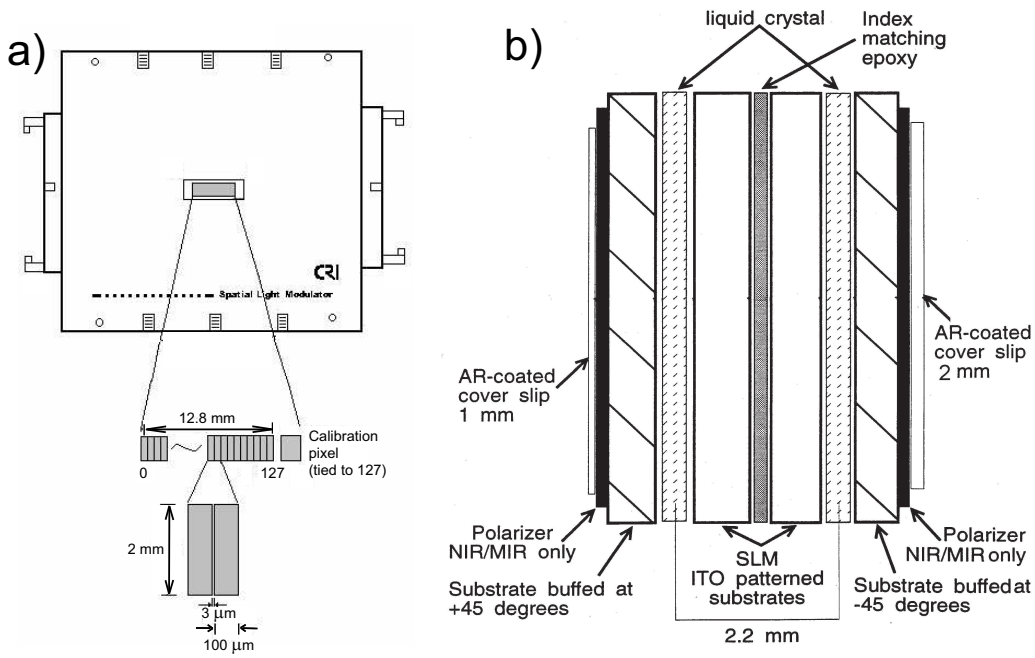

Figure 3.2: The SLM-256 amplitude/phase masks: a) front view. The pixel dimensions are given as well; b) side view of only the SLM masks. The drawing contains the polarizers (NIR/MIR stands for Near InfraRed or Middle InfraRed, AR for Anti-Reflective coating), the glass plates together with the $\pm 45°$ buffing directions, the liquid crystal layers, the ITO electrodes and the index matching epoxy [34].

drive voltage with a 12 bit resolution controlled by a GPIB interface. Alternating current is required in order to avoid electromigration effects in the LC.

If the SLM is placed in the Fourier plane of a dispersion-free compressor (see section 3.2.4), the frequency components can be delayed and/or attenuated towards each other.

A typical array is shown in Figure 3.3. It is electronically addresses and allows continuously variable phase control of each pixel. Moreover, it allows programmable control of the pulse shape within 200 milliseconds.

3.2.3 The SLM-1280

During this work, CRI Inc. has constructed a new SLM unit which consists of two arrays of 640 pixels each.

With a higher number of pixels, the spectral resolution and modulation depth are considerably improved with respect to the SLM-256 model. This al-

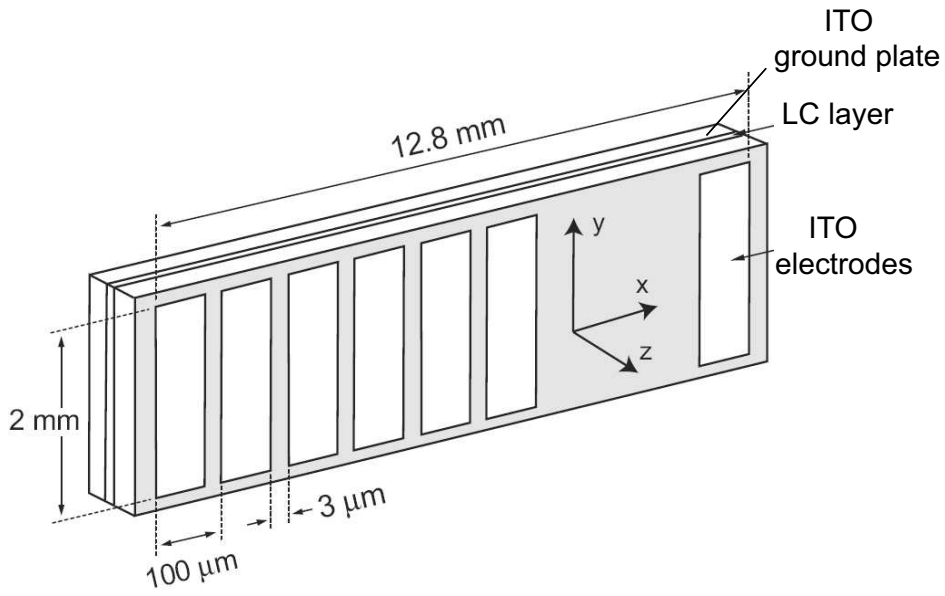

Figure 3.3: Scheme of a filtering mask based on a liquid crystal array. In the SLM-256 there are two of these masks. The dimensions and position of the pixels is given as well.

lows one to resolve sharper peaks in the spectra of the optimal pulses obtained in feedback control experiments. The SLM 1280 is now able to compensate larger chirps, to predefine pulse trains with larger temporal distances. This will improve the previous work on parametric optimization experiments.

One pixel is 5 mm high and 98 μm wide. The interpixel gap amounts 2 μm. The total aperture of the SLM mask is 64 mm. The overall size of the SLM unit is 165 $\times$ 305 $\times$ 33 mm. The electronic driver provides voltages between 0 and 10 V with a 12 bit resolution and is controlled by a RS-232 or an USB interface. All the electronics, the SLM masks and cabling are situated in a single housing. The working spectral range is 488–900 nm, due to chosen the NIR polarizers. The response time of the LC fluid is about 35 ms [35].

The transmission and the damage threshold of the LC cells and of the polarizers were measured in the frame of the present work. For pulses with peak intensities between 0.1–630 GW cm^{-2} corresponding to 0.3–300 μJ cm^{-2} in the spectral region of 490–833 nm no damage of the LC cells was observed after three hours of exposure. For the employed wavelengths, the transmission was measured to be about 70–80 %. (The absorbtion of frequency-doubled photons of 390 nm emerging the femtosecond amplifier lead to an instantaneous damage of the LC cells at an energy density of only 1 μJ cm^{-2}.)

An interesting feature of the SLM unit is the optional reflective mode.

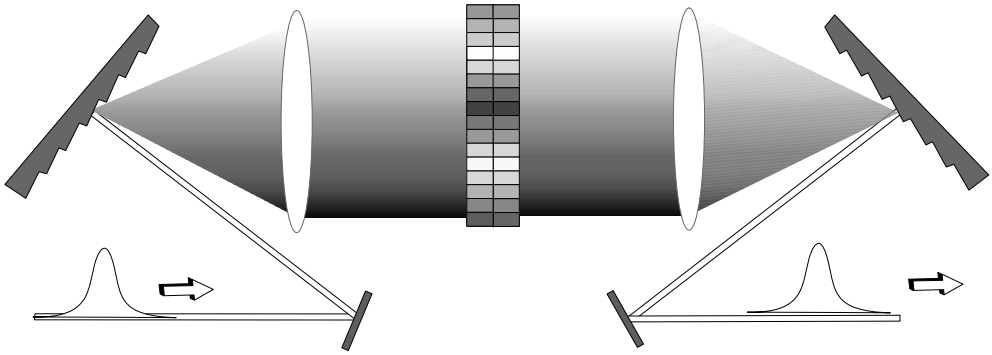

Figure 3.4: The dispersion-free compressor: two gratings and two lenses separated by the focal length of the lens *f*. The spectrum can be modulated if in the symmetry plane (Fourier plane of the lens) a filtering mask is situated, based on liquid crystals, e.g. the SLM. If the modulator does not work the outgoing pulse has the same properties as the incoming pulse.

By removing the second polarizer at the output face of the SLM, a mirror can be placed so the light passes twice through the system. In this way, the polarizer at the entrance face of the unit acts as both polarizer for the light entering and leaving the SLM. According to Ref. [35], this feature doubles the action of the SLM resulting in a faster time response between switching the drive settings and allows a greater phase modulation. The pulse shaper has not been yet tested in the reflective mode.

3.2.4 The Pulse Shaping Apparatus

This section focuses on the setup used in this work in order to modulate femtosecond laser pulses, i.e. the spectral electric field. The most important component, the programmable spatial light modulator (SLM) based on two arrays of LC was described in section 3.2.2.

In Chapter 2 the principle of a femtosecond pulse compressor was shown (Figure 2.6b). It consists of two or four diffraction gratings[7]: the first disperses the femtosecond pulse into its frequency components, which travel different optical paths; due to its geometrical positioning, the second grating collimates the frequencies, which are recombined by the third and fourth gratings. By varying the distance between the first and the second, and respectively the third and the fourth grating one can generate different linear negative chirps [14]:

[7]Four diffraction gratings ar needed to compensate the spatial chirp.

$$\left.\frac{d^2\psi}{d\omega^2}\right|_{\omega_0} = -\frac{4\pi^2 c}{\omega_0^3 d^2 cos^2\big(\theta_{out}(\omega_0)\big)} \cdot l \tag{3.21}$$

where l is the distance between the first and second grating, d is the grating constant and $\theta_{out}(\omega_0)$ is the diffraction angle of the grating at the central frequency ω_0. For economic reasons a mirror can be used in the center of the setup and only the first two gratings are used. The chirp sign is given by the angular dispersion of the grating. The pulse compressor is mainly used to compensate the phase modulation (linear positive chirp) introduced by other dispersive elements (optical glass).

By combining two gratings and two lenses (in a telescopic arrangement), one can obtain a setup which generates larger positive or negative chirps [36]. The first grating spectrally disperses the femtosecond pulse. The frequencies are parallelized by the first lens, which Fourier transforms the pulse from the time domain into the spectral domain. In the Fourier plane of the lens the spectral components are spatially separated along one dimension [37]. They are focused by the second lens onto the second grating. An inverse Fourier transform into the time domain takes place after passing the second lens.

If all the optical elements are symmetrically separated by the focal length of the lenses f, the pulse leaving the setup has the same characteristics as the pulse entering the setup. Since no phase modulation occurs, the setup is called a zero-dispersion compressor (see Figure 3.4). This dispersion-free condition takes into account that the lenses are thin and free of chromatic aberrations. For pulses shorter than 20 fs, these effects can become important [38].

Femtosecond pulse shaping technique by using a LC modulator was first pioneered by A. Weiner and co-workers [38]. Other pulse shaping techniques were developed in the past years. A brief overview is given at the end of this chapter in section 3.3.

In this work two setups were used: a linear and a folded one. In the linear $4f$-setup used in this work (displayed in Figure 3.4) the gratings have 1200 lines/mm. The individual frequencies are focused in the x-plane, whereas in the y-plane remain unfocused. Thus cylindrical lenses are required (here $f = 200$ mm) in order to avoid damaging the polarizers in the SLM. If the lenses are not separated by $2f$ the beam is divergent and a temporal chirp leaves the setup. If the gratings are not situated exactly in the focal plane of the lenses, an additional spectral chirp[8] is generated. This distorts the temporal phase of the pulse and can not be compensated.

The height of the LC layer amounts 2 mm (see Figure 3.3). Hence, the beam diameter at the entrance in the pulse shaper setup has to be around

[8]The frequencies are spatially separated within the laser beam profile.

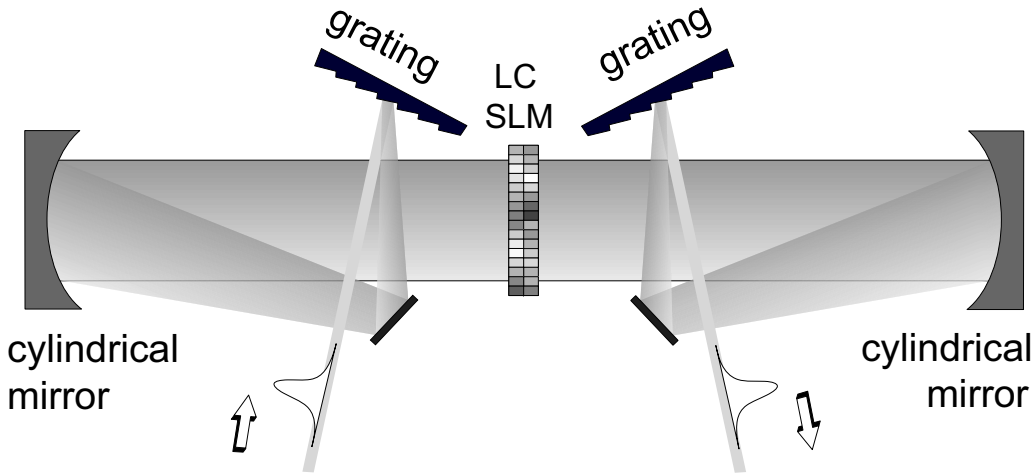

Figure 3.5: The dispersion-free folded setup: two gratings and two lenses separated by the focal length of the lens *f*. The spectrum can be modulated if in the symmetry plane (Fourier plane of the lens) a filtering mask is situated, based on liquid crystals, e.g. a Spatial Light Modulator.

2 mm, too. A telescope can be used to reduce the laser beam diameter. More about the alignment of the pulse shaping apparatus can be found in Appendix A.

After the frequency components were dispersed by the grating and collimated by the first lens, it was possible to determine how much of the spectrum covers the modulator active mask. For 770 nm it was measured 0.342 nm/pixel and for 833 nm, 0.330 nm/pixel, respectively.

The linear setup was used for the experiments on alkali metal clusters described in Chapter 8 and 9 with the femtosecond laser system described in Chapter 4, section 4.2.1, which provides laser pulses with a spectral bandwidth of up to $\Delta\lambda = 10$ nm at FWHM. The intensity of the laser beam after passing through the linear configuration decreases with 40 %.

For pulses with larger bandwidth (up to $\Delta\lambda = 35$ nm at FWHM) provided by the laser system described in Chapter 4, section 4.2.2 the folded setup was used (see Figure 3.5). In this way the experiments on the organometallic system, described in Chapter 6, section 6.4, could be performed. The grating constant is 600 lines/mm and the cylindrical lenses were replaced with cylindrical plane concave mirrors with $f = 150$ mm. Their inner concave side was covered with a dielectric layer, leading to a reflectivity of 99 %. The overall intensity losses of the folded setup are about 25 %. The *off-axis* aberration caused by the diffraction of the spectrum by the grating onto the cylindrical mirrors is minimized by the two folding mirrors (see Figure 3.5).

In the case of the SLM-1280 model, because of the larger aperture of the pixel mask, the linear setup is slightly modified. The gratings were chosen with 2100 lines/mm, but the cylindrical lenses were not replaced ($f = 200$ mm). This linear $4f$-setup permits the covering of 50–55 mm of the SLM mask. In order to cover all the pixels the linear pulse shaping apparatus has to contain lenses with longer focal lengths, which would considerably prolong the setup (in transmission mode). In reflective mode a grating which disperses the spectrum and a lens which collimates the frequencies onto the SLM-1280 mask assure an operating pulse shaping apparatus. In this case a careful alignment is required.

3.2.5 Phase and Amplitude Modulation

The programmable LC modulator used in this work is capable of both phase and amplitude modulation simultaneously and independently. The two LC arrays are bonded together at approximately 2.2 mm distance [34]. In our setup the initial vertical polarization of the laser beam is changed before the first grating by a $\lambda/2$ wave-plate with 90°. The incident light is now horizontally polarized to assure a parallel polarization with the extraordinary axis of the LC (x-axis) at the input face of the SLM. At the output face of the modulator, a polarizer selects only the horizontally polarized light [35]. (After leaving the pulse shaping apparatus, i.e. the second grating, the polarization is changed back.) The orientation of the LC crystal molecules is orthogonal to another and 45° to the polarization of the incoming light. The LC mask behaves now like a (electrically variable) waveplate.

From the equations (3.19) and (3.20) the retardance varies the polarization depending on the applied voltage $\Delta\phi_i(V) = 2\pi\Delta n(V)d/\lambda$ for the i-th pixel, at a given LC crystal thickness and central wavelength.

After the polarization of the input light field is horizontally rotated and passes through the first LC array (A), as depicted in Figure 3.6. The polarization is rotated in direction $\boldsymbol{a}$ (see inset in Figure 3.6) according to the phase retardance $\Delta\phi^{(A)}$. By passing through the second LC array (B), voltage-dependent phase retardance $\Delta\phi^{(B)}$ occurs and the other polarization component is rotated in the other direction $\boldsymbol{b}$ in the second LC array. Hence the phase retardance between the two perpendicular components ($\boldsymbol{a}$ and $\boldsymbol{b}$) can be compensated. The polarization direction can be also rotated in such a way that the attenuation is compensated while the phase shifts. The exponential of the average phase retardance $\frac{\Delta\phi^{(A)}+\Delta\phi^{(B)}}{2}$ gives the phase shift. The amplitude is altered according to the cosine of the differential retardance $\Delta\phi^{(A)} - \Delta\phi^{(B)}$ (see equation (3.22)).

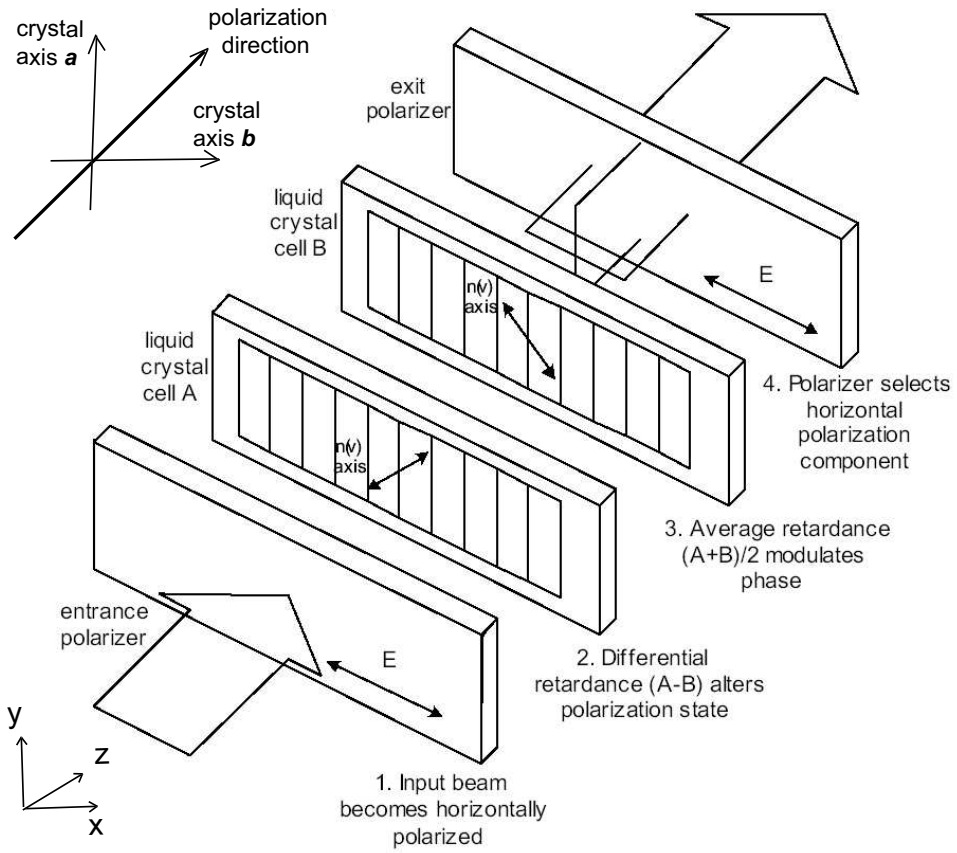

Figure 3.6: Scheme of phase and amplitude modulation. The incident light is polarized in the horizontal x direction. The two LC molecules in the two arrays are rotated with 45° with respect to the x axis and have an angle of 90° with respect to each other [35]. The inset shows how the input polarization is split in two perpendicular components: along the fast crystal axis ***a*** and ***b***.

The output electric field E_n^{output} of the n^{th} pixel after leaving the modulator can be written as [39]

$$E_n^{output} = E_n^{input} \cdot \underbrace{\cos\big((\Delta\phi^{(A)} - \Delta\phi^{(B)})/2\big)}_{\text{Amplitude modulation}} \cdot \underbrace{\mathrm{e}^{i(\Delta\phi^{(A)}+\Delta\phi^{(B)})/2}}_{\text{Phase modulation}} = E_n^{input} \cdot R_n \tag{3.22}$$

with $R_n = e^{i\psi(\omega)} \cdot \sqrt{T_n(\omega)}$ as filter function applied to the n^{th} pixel; $T_n(\omega)$ is the transmission and $\psi_n(\omega)$ is the phase filter of each element. For $\psi(\omega) = 0$ the spectral filter function allows amplitude-only modulation, whereas for $T_n(\omega) = 1$ the filter function can modulate only the phase mask.

Pure phase modulation is achieved when the cosine in expression (3.22) is equal to 1. Amplitude modulation is also accompanied by a phase modulation [39]. As the SLM-256 posses two LC arrays, the second one compensates for the unwanted phase modulation so that pure intensity attenuation of the optical waveform is obtained.

None of the two masks is able to modulate alone the phase or the amplitude but their combination allows independent phase and amplitude modulation.

3.2.6 Calibration

The refractive index n(V) of the LC molecules is voltage-dependent. The resulting phase retardance for both arrays $\Delta\phi^{(A)}$ and $\Delta\phi^{(B)}$ depends also on the applied voltage on each pixel of each array. For an optimal operation of the SLM mask, the dependence $\Delta\phi^{(A,B)}(V)$ has to be determined experimentally (calibration). From the equation (3.22) one can calculate the transmission filter

$$T = \cos^2\big(\frac{1}{2}(\Delta\phi^{(A)} - \Delta\phi^{(B)})\big) \tag{3.23}$$

and the phase filter

$$\psi = \frac{1}{2}(\Delta\phi^{(A)} + \Delta\phi^{(B)}) \tag{3.24}$$

for each pixel of the two arrays.

Taking the previous two equations into account the phase retardances for the two arrays A and B can be written

$$\Delta\phi^{(A)} = \frac{\pi}{2} + \psi + \arccos\sqrt{T} \tag{3.25}$$

$$\Delta\phi^{(B)} = \frac{\pi}{2} + \psi - \arccos\sqrt{T} \tag{3.26}$$

where a factor $\frac{\pi}{2}$ is added in order to avoid negative phase retardances, which are physically impossible.

Hence the phase retardances of each array are functions of the transmission and the phase filter on each stripe. But the retardance is also a function of wavelength (see equation (3.19)).

The calibration procedure implies the plotting of the transmission versus the applied voltage. This is recorded for each array.

The experimental setup for calibrating the SLM is discussed below. A power meter (or a photodiode) is situated behind the SLM mask or after the second grating. The array A is set to maximum transmission, while the

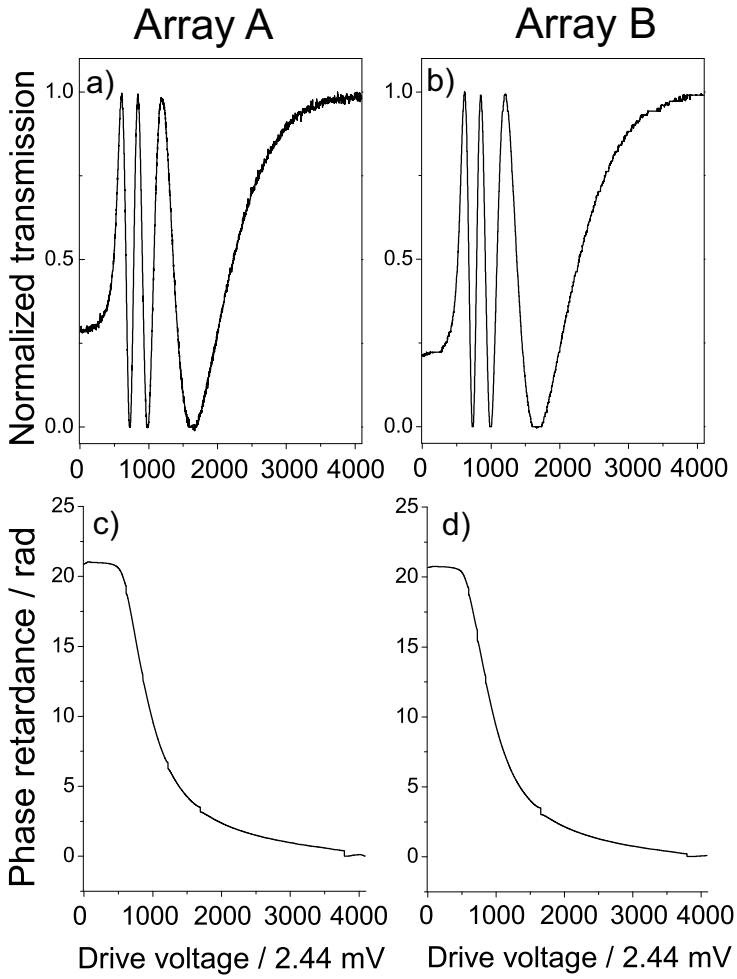

Figure 3.7: The calibration of the SLM implies the dependence between the phase retardance and the applied voltage for both LC arrays. By setting one array to $V_{\max} = 10$ V, corresponding to 4096 drive voltage steps of each 2.44 mV, the voltage-dependent transmission for the other array is measured (a) and (b). The calibration function for each of the arrays A and B is shown in (c) and (d) respectively. The curves were recorded at 833 nm laser central wavelength.

voltage on array B is varied through all 4096 possible drive voltages. The overall transmission can be measured with the power meter or the photodiode and recorded by a PC. The procedure is repeated for the array A, while the transmission of array B is set to maximum (see Figure 3.7).

Using the equations (3.25) and (3.26) predefined pulse shapes can be produced.

3.2.7 Limitations of the SLM

The Nyquist Limit

The Nyquist Limit is maybe the most important limitation cause of the SLM. It originates from the sampling theorem and concerns pulse trains with subpulses separated by a large time interval. The Nyquist sampling theorem states that the phase difference between two adjacent pixels should not be larger than π:

$$\delta\psi < \pi. \tag{3.27}$$

For the present setup it was calculated that for the linear phase modulation

$$\psi(\omega) = b_1(\omega - \omega_0) \tag{3.28}$$

with the discretization phase function (which leads to a frequency shift)

$$\psi_n(\omega) = b_1\delta\omega(n - \frac{N}{2}), \quad with \quad n \in 0, \cdots, N = 128 \tag{3.29}$$

the replica of the same pulse appear after

$$b_{1,\max} = \left(\frac{\delta\psi}{\delta\omega}\right)_{\max} = \frac{\pi}{\delta\omega} = \frac{1}{2\delta\nu} = \frac{1}{2}\Delta t^{\text{pulse}}_{\text{replica}} \tag{3.30}$$

where $\Delta t^{\text{pulse}}_{\text{replica}}$ is the time separation between the pulse replica. At 770 nm $b_{1,\max} = 2.89$ ps [20] and at 833 nm $b_{1,\max} = 3.5$ ps [40] (whereas $\delta\lambda = 0.342$ nm/pixel).

The quadratic phase function has the form

$$\psi(\omega) = \frac{1}{2!}b_2(\omega - \omega_0)^2 \tag{3.31}$$

whereby the discretization function leads to a linear phase:

$$\psi_n(\omega) = \frac{1}{2!}b_2\delta\omega^2(n - \frac{N}{2})^2, \quad with \quad n \in 0, \cdots, N = 128. \tag{3.32}$$

Then the quadratic Taylor coefficient is

$$b_{2,\max} = \left(\frac{2\delta\psi}{\delta\omega^2}\right)_{\max} = \frac{2\pi}{(N-1)\delta\omega^2} = 4.2 \cdot 10^4 \text{ fs}^2. \tag{3.33}$$

The maximal values of the Taylor coefficients play an important role in pulse shaping. For example, if N increases (the case of SLM-1280) the maximal values of the Taylor coefficients increase (for the same spectral broadness) which leads to a better capability of the pulse shaper to compensate larger chirps. If N remains constant, but $\Delta\lambda$ (at FWHM) increases, the maximal values of the Taylor coefficients decrease. The temporal resolution increases as well.

Pixelation Effects

When voltage is applied on each pixel, all the LC molecules will align themselves along the direction of the electric field, except those who are in the vicinity of the glass plates (see Figure 3.1b). This is because the elastic force at the glass plates' surface resist the tilting motion [41]. If an exact pulse shape is desired this effect is observable as small imperfections between the desired and the measured shape.

Other effects are due to the gaps between two neighboring pixels. When a linear spectral phase is applied with $\delta\psi$ constant between two adjacent pixels, due to the discretization of the pixel mask, the output pulse is not only the convolution of the input pulse with the desired impulse response function, but also with a series of replica impulse response functions [37]. The resulting pulse replica appear at temporal distances $\Delta t = m\frac{\delta\psi}{\delta\omega}$. ($m \in \mathbb{N}$ and $\delta\psi$ is the angular frequency difference between two adjacent pixels). An effect, however negligible for $\Delta\lambda = 10$ nm (at FWHM), observed in Ref. [39], is due to the nonlinear distribution of frequencies in the Fourier plane where the LC SLM is located. Smoothing effects due to the gaps between two neighboring pixels slightly modify the phase function since the LC molecules situated in the gaps do not permit abrupt phase changes [40]. A linear phase function would then be smoothed.

3.3 Examples of Other Pulse Shaping Techniques

Acousto-Optic Modulators

Acousto-optic modulators (AOM) can be used as well for phase and amplitude shaping of femtosecond laser pulses. The AOM can be set also in the Fourier plane of a zero-dispersion compressor in a $4f$-arrangement, like described at the beginning of the section. The first demonstration of pulse shaping by using an AOM was performed in the group of Warren [42, 43]. The AOM crystal (typically TeO_2) is driven by an radio-frequency signal which is converted into a travelling acoustic wave by a piezoelectric transducer. The acoustic wave travels across the modulator leading to a refractive index grating through the photo-elastic effect. The spatially dispersed spectrum of the laser pulse is changed according to the grating spatial modulation function. The strength of the acoustic wave relates with the amplitude of the diffracted light, whereas the phase of the acoustic wave is the phase change of the diffracted light. The main advantages of using an AOM to modulate fem-

tosecond laser pulses is the high effective pixel density (approx. 2000 pixels for a 4 cm crystal [42]). The switching time is relatively fast (microsecond time scale) and no calibration is necessary. There are some disadvantages: acoustic nonlinearities (usually frequency, intensity and material dependent, which are particularly strong in TeO_2), off-grating diffraction losses, low diffraction efficiency (about 40 %, according to Ref. [44]). Timing is very critical as well: since the acoustic wave leaves the modulator, the modulation time is limited by the time needed for the wave to travel across the crystal. The femtosecond laser pulse and the acoustic wave must also match exactly in the modulator. Moreover, AOMs are not suitable for lasers with high repetition rates, since the pulse shape would change from pulse to pulse [44].

Deformable Mirrors

Deformable mirrors are used to manipulate only the phase of a laser pulse. The phase shift is related to the degree of deflection [45]:

$$\Delta\phi = 2 \cdot \frac{2\pi\Delta z}{\lambda} \tag{3.34}$$

The deformable mirrors used by Heritage and co-workers [45] allowed the control of the third-order spectral phase, but not programmable pulse shaping. They applied equal and opposite pressure at each end point of a thin mirror, which bent into a S-shape. There are two types of deformable mirrors: (i) a very thin membrane situated over an electrode array and (ii) a glass substrate glued over an array of piezoelectric elements [45].

Recently, the use of micro-machined membrane deformable mirrors was reported [46]. The silicone nitride membrane was suspended over a set of electrodes. Applying a potential between the electrodes and the membrane, the electrostatic attraction force deforms the mirror surface. This deviation from the flat mirror surface permits the light to travel a different optical path. As a result, the phase of the frequency components is modified depending on the deformation area.

Static Masks

The static masks were the first pulse shapers with predefined phase and amplitude. They were initially used in stretchers [47]. Since $H(\omega)$ is fixed for every mask, for every desired shape E_{output} a new mask with different $H'(\omega)$ needs to be constructed. They are useful if the duration of the input pulse is much shorter than the duration of the desired output pulse. The input field can be considered as a delta function with a constant spectrum, the modulation function is then $H(\omega) = E_{output}$. Static masks are also used for creating

	Phase Mod.	Ampl. Mod.	Discre-tization	Program-mable	Switch Time	Efficiency
Static Masks	Yes	Yes	None	No	Impos-sible	High
AOM	Yes	Yes	$\sim$ 2000	Yes	μs	$\sim$ 40%
Deform. Mirrors	Yes	No	$\sim$ 39	Yes	$\sim$ 1 ms	High
LCD	Yes	Yes	$\sim$640	Yes	$\sim$35-200 ms	High

Table 3.1: Comparison between different pulse shaping techniques (taken from [46]).

pulse trains. By microlithography techniques, substrates can be engraved creating phase masks. For example, if the phase mask contains alternating π shifts, the output is a tailored pulse with close spaced subpulses [48]. Static masks are used in femtosecond amplification techniques rather than in programmable pulse shaping.

Comparison Between Different Pulse Shaping Techniques

In the Table 3.1 the most popular pulse shaping techniques are compared. Discretization means either the number of pixels (or of the actuators) intersected by the laser field. Switch time is how fast the shaper changes its modulation.

From the aforementioned pulse shaping devices and the comparison given in Table 3.1 it can be concluded that AOMs are serious competitors of the LC modulators. Nevertheless the latter ones are widely preferred in femtosecond pulse shaping laboratories. One of the reasons is that the AOM transmission is diminished by the low diffraction efficiency in the crystal, which leads to losses of the pulse intensities, hence the use of highly transmittable SLM is of an advantage. Another reason is the relatively high damage threshold of the LC; thus femtosecond amplifiers can be used with SLMs. The LC masks are recommended for femtosecond oscillators with high repetition rates, since there is no critical timing with an acoustic wave travelling through the modulator. Another advantage of the pulse shaping with LC modulators is that the alignment of such a pulse shaping apparatus is quite uncomplicated.